Controlling Quantum Devices with Nonlinear Hardware

I. N. Hincks

Department of Applied Math, University of Waterloo, Waterloo, Ontario N2L 3G1, Canada
and Institute for Quantum Computing, Waterloo, Ontario N2L 3G1, Canada

C. E. Granade

School of Physics, University of Sydney, Sydney, New South Wales 2052, Australia
and Centre for Engineered Quantum Systems, Sydney, New South Wales, Australia

T. W. Borneman

Department of Physics, University of Waterloo, Waterloo, Ontario N2L 3G1, Canada
and Institute for Quantum Computing, Waterloo, Ontario N2L 3G1, Canada

D. G. Cory

Department of Chemistry, University of Waterloo, Waterloo, Ontario N2L 3G1, Canada;
Institute for Quantum Computing, Waterloo, Ontario N2L 3G1, Canada;
Perimeter Institute for Theoretical Physics, Waterloo, Ontario N2L 2Y5, Canada
and Quantum Information Science Program, Canadian Institute for Advanced Research,
Toronto, Ontario M5G 1Z8, Canada

High-fidelity coherent control of quantum systems is critical to building quantum devices and quantum computers. We provide a general optimal control framework for designing control sequences that account for hardware control distortions while maintaining robustness to environmental noise. We demonstrate the utility of our algorithm by presenting examples of robust quantum gates optimized in the presence of nonlinear distortions. We show that nonlinear classical controllers do not necessarily incur additional computational cost to pulse-optimization, enabling more powerful quantum devices.

I. INTRODUCTION

The ability to coherently control the dynamics of quantum systems with high fidelity is a critical component of the development of modern quantum devices, including quantum computers [1], actuators [2,3], and sensors [4–6], that push beyond the capabilities of classical computation and metrology. In recent years, quantum computation has presented a compelling application for quantum control, as high-fidelity control is essential to implementing quantum-information processors that may achieve fault tolerance [7–9]. As quantum devices continue to grow in size and complexity, the requirements of classical control hardware also increase. This will more frequently produce situations with a significant trade-off between hardware-response simplicity and overall hardware capability.

The performance of numerically optimized quantum gates in laboratory applications strongly depends on the response of the classical electronics used to apply the control sequence. In this article, we provide a formalism for including arbitrary classical hardware models into pulse-finding algorithms such that the produced control sequences are tailored to work robustly for the intended hardware controllers. A novelty of our general framework is the ability to natively incorporate nonlinear and noninvertible

hardware behavior. Importantly, it also naturally allows for robustness against uncertainties and errors in parameters describing the hardware, in contrast to previous methods which dealt only with Hamiltonian parameters such as overall power and offset frequency [10–12].

Recently, it was demonstrated how a model of linear distortions of the control sequence, such as those arising from finite bandwidth of the classical control hardware, may be integrated into optimal-control-theory (OCT) algorithms [13–16]. We generalize and extend these methods to admit hardware models which are noninvertible or nonlinear, allowing the experimenter to maximize control efficiency and measurement sensitivity by driving hardware performance to its limits without sacrificing the ability to perform robust, high-fidelity quantum control.

Our framework includes a complete integration of the system-apparatus dynamics and models hardware components explicitly, such that their effect on a quantum system can be computed and compensated for using numerical OCT [17] algorithms to optimize control sequences. Control sequences designed using OCT algorithms, such as the gradient-ascent-pulse-engineering (GRAPE) [18] algorithm, can be made robust to a wide variety of field inhomogeneities, pulse errors, and noise processes [19–21].

These methods are also easily extended [22–25] to other applications and may be integrated into other protocols [26].

We begin developing our method generally, without making assumptions about the device of interest, so that our results may be broadly applicable to a wide range of quantum devices. We briefly discuss how our theory is easily applied to any linear distortion, and then in more detail, demonstrate with numerics how nonlinearities in control hardware may be included. As an example, we derive high-fidelity control pulses for strongly driven superconducting resonators exhibiting nonlinear kinetic inductance [27–29], that are robust to uncertainty in the amount of nonlinearity present. While our methods apply generally to a wide range of quantum control modalities, superconducting resonators serve well as an illustrative test bed of our method's utility, having found significant recent application in pulsed electron spin resonance [30–32] and circuit QED to increase induction measurement sensitivity and provide an interface for microwave photon quantum memories [33,34].

II. SETUP

With this goal in mind, we review the problem of controlling a quantum system [35]. Given a system Hamiltonian

$$H(t) = H_0 + \sum_{l=1}^{L} q_l(t) H_l \qquad (1)$$

acting on a Hilbert space of dimension d, where H_0 is the internal Hamiltonian and $\{H_l\}_{l=1}^{L}$ are the control Hamiltonians, how do we choose the envelopes $\{q_l(t)\}_{l=1}^{L}$ such that at time T we effect the total unitary U_{target}? A well-known result in quantum control theory tells us that such envelopes exist for any target unitary U_{target} whenever the span of the nested commutations of the Hamiltonians $\{H_l\}_{l=0}^{L}$ is at least $d^2 - 1$ [35]. Actually, finding these envelopes is the goal of OCT. We focus our attention on numerical optimization methods.

It will be clear that the framework we construct will be compatible not only with the problem of generating a full unitary operation as outlined above, but all similar problems such as state-to-state transfers, expectation values over static distributions, open system maps, etc.

The functions $\{q_l(t)\}_{l=1}^{L}$ seen by the quantum system Hamiltonian represent a distorted version of what was actually input to the classical hardware. Effects such as circuit transfer functions, mixer imbalance, noise, amplifier nonlinearity, and cross talk will all contribute to this distortion acting on the input pulse. Since we are ultimately interested in doing numerics, we begin by discretizing the time domain and therefore model all relevant hardware by what we will call a *discretized distortion operator*. This is a
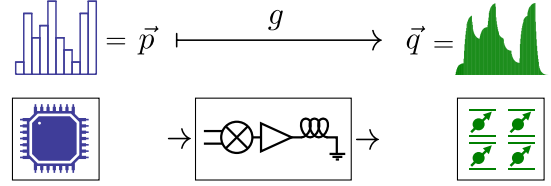

FIG. 1. An illustration depicting the action of the distortion operator g on the input pulse $\vec{p}$.

function $g: \mathbb{R}^N \otimes \mathbb{R}^K \to \mathbb{R}^M \otimes \mathbb{R}^L$, which takes an input pulse sequence $\vec{p}$ with some associated time step dt, and outputs a distorted version of the pulse $\vec{q} = g(\vec{p})$, with an associated time step δt. $\vec{p}$ is the pulse as stored in the experimenter's computer, and $\vec{q}$ is the pulse generating the Hamiltonian seen by the quantum system, as illustrated in Fig. 1.

The integers N and M are the number of input and output time steps, respectively, and K and L are the number of input and output control fields, respectively. In the case of on-resonant quadrature control of a qubit, $K = L = 2$. We omit subscripts on the time steps dt and δt for notational simplicity; uniform time discretization is not required. Typically, we will have $\delta t < dt$ to allow for an accurate simulation of the quantum system. The condition $M \delta t = N dt$ need not hold, for example, $M \delta t > N dt$ will be useful when the distortion has a finite ringdown time.

The discretized distortion operator g will often derive from a *continuous distortion operator* $f: \mathbf{L}_1(\mathbb{R}, \mathbb{R}^K) \to \mathbf{L}_1(\mathbb{R}, \mathbb{R}^L)$, which takes a continuous input pulse $\alpha(t) = \{p_1(t), \ldots, p_K(t)\}$ and outputs a distorted pulse $\beta(t) = \{q_1(t), \ldots, q_L(t)\}$ given by $f[\alpha](t)$. The discretized version is obtained by composing f on either side by a discretization and dediscretization operator $g = f_1 \circ f \circ f_2$ (examples of this are provided in the Supplemental Material [36]).

We can compute the effect that an input pulse $\vec{p}$ has on the quantum system by first computing $\vec{q} = g(\vec{p})$, and then using the piecewise constant solution to Schrödinger's equation. That is, in each of the individual M-output time steps, we may solve Schrödinger's equation with a constant Hamiltonian to give us the unitary propagator corresponding to the mth time step

$$U_m(\vec{q}) = \exp\left[-i\,\delta t \left(H_0 + \sum_{l=1}^{L} q_{m,l} H_l\right)\right] \qquad (2)$$

so that the total propagator from $t = 0$ until $t = M \delta t$ is given by

$$U(\vec{q}) = \prod_{m=1}^{M} U_m(\vec{q}), \qquad (3)$$

where multiplication is ordered so that the first time step appears at the far right. If the internal Hamiltonians $\{H_l\}_{l=0}^{L}$

are time dependent, more complex solutions may be used [16].

We can now incorporate the distortion operator g into standard methods from optimal control theory. In particular, we focus on the GRAPE algorithm [18], though we again stress that using other algorithms would work as well, especially noting that those algorithms which make use of gradients of the objective function may continue to do so [39–41]. To begin, consider the unitary objective function

$$\Phi[\vec{q}] = |\mathrm{Tr}[U_{\mathrm{target}}^{\dagger} U(\vec{q})]|^2/d^2, \qquad (4)$$

which outputs values in the range [0, 1] and achieves the maximum value 1 if and only if the pulse $\vec{q}$ generates a unitary $U(\vec{q})$ that is equal to U_{target} up to global phase. Penalties can be added to this basic objective function in order to demand that the solution admit certain properties. For instance, penalty functions have been used to ensure robustness to control noise and limited pulse fluence [20,42–44] or to ensure that undesired subspaces are avoided [45,46].

Now we include the effect of our hardware by modifying the objective function to compose with the distortion operator

$$\Phi_g[\vec{p}] = \Phi \circ g(\vec{p}), \qquad (5)$$

which gives us a measure of the quality of an input gate $\vec{p}$. As with standard GRAPE, we ascend this objective function to the nearest local maxima starting with a random initial guess and choosing an uphill direction based on the gradient of Φ_g with respect to the components of $\vec{p}$. In the examples that follow in later sections, we use a standard adaptive step-size conjugate-gradient routine implemented in the QUANTUMUTILS for *Mathematica* library [47]. In practice, with standard GRAPE, a surprising fraction of local maxima are globally optimal when using experimentally relevant Hamiltonians and parameters.

Using the multivariable chain rule, we compute the gradient of Φ_g to be

$$\nabla_{\vec{p}}(\Phi_g) = \nabla_{g(\vec{p})}(\Phi) \cdot J_{\vec{p}}(g), \qquad (6)$$

$$[J_{\vec{p}}(g)]_{m,l,n,k} = \frac{\partial g_{m,l}}{\partial p_{n,k}}, \qquad (7)$$

thus separating the objective function derivatives into the derivatives of the distortion operator alone, and the quantum evolution alone. Here, the dot represents a contraction over the indices m and l, and $J_{\vec{p}}(g)$ is the Jacobian of g at $\vec{p}$.

Though evaluating $\nabla_{g(\vec{p})}(\Phi) = [\partial\Phi/\partial q_{m,l}]_{m,l}$ naively would require simulating the action of ML pulses, the GRAPE algorithm provides an expression for this gradient in terms of the time-step unitaries $U_m(\vec{q})$ that are already computed when evaluating $\Phi(\vec{q})$,

$$\frac{\partial\Phi}{\partial q_{m,l}} = -2\mathrm{Re}[\langle P_m|i\,\delta t H_l X_m\rangle\langle X_m|P_m\rangle], \qquad (8)$$

where $P_m := (\prod_{i=m+1}^{M} U_i^{\dagger})U_{\mathrm{target}}$, $X_m := \prod_{i=m}^{1} U_i$, and $\langle A|B\rangle = \mathrm{Tr}(A^{\dagger}B)$ is the trace inner product.

Therefore the only remaining challenge is to compute the Jacobian $J_{\vec{p}}(g)$. This task depends entirely on the specific nature of the discrete distortion operator g. For instance, if g is linear, then computing the Jacobian tensor is in principle trivial, and is independent of the input pulse $\vec{p}$. In the examples that follow, as well as many examples found in the Supplemental Material [36], Secs. A–C, the components of this Jacobian tensor will be worked out in detail.

Because the cost of evaluating g will typically not grow more than polynomially with the number of qubits, the computational cost of the optimization effectively remains unchanged from standard GRAPE, as it is still dominated by the cost of computing the M matrix exponentials.

Although we have singled out the GRAPE algorithm as our routine to optimize the objective function, this choice is based largely on the favorable convergence properties of the algorithm [48], and does not prevent the use of a different routine. In particular, GRAPE is a greedy algorithm which attempts to find an optimum closest to the initial value by choosing a direction related to the steepest uphill slope. Global optimizers such as Nelder-Mead, genetic algorithms, or hybrid gradient algorithms [26,48–50] could be used without modification by substituting the usual objective function Φ with the distortion-modified objective function Φ_g. Such methods are useful in cases where the control landscape is known to be saturated with suboptimal maxima. Gradient-free methods may be advantageous in cases where it is difficult or overly expensive to compute the Jacobian tensor of Φ_g.

III. CONVOLUTION EXAMPLE

Making use of the abstract formalism described above, our first example is the continuous distortion operator given by the convolution with an LK kernel $\phi(t)$,

$$\beta(t) = f(\alpha)(t) = (\phi \star \alpha)(t) = \int_{-\infty}^{\infty} \phi(t-\tau) \cdot \alpha(t) d\tau. \quad (9)$$

The convolution kernel ϕ models any distortion that can be described by a linear differential equation, such as a simple exponential rise time, control-line crosstalk, or the transfer function of the control hardware [13,14,51,52]. We compute the discretized distortion operator to be

$$q_{m,l} = \sum_{n=1,k=1}^{N,K} \left(\int_{(n-1)\,dt}^{n\,dt} \phi_{l,k}((m-1/2)\,\delta t - \tau)\,d\tau \right) p_{n,k}, \qquad (10)$$

where we see that it acts as a linear map

$$\vec{q} = g(\vec{p}) = \tilde{\phi} \cdot \vec{p}, \qquad (11)$$

where we are contracting over the n and k indices with the components of the tensor $\tilde{\phi}$ given by the integrals

$$[\tilde{\phi}]_{m,l,n,k} = \int_{(n-1)\,dt}^{n\,dt} \phi_{l,k}((m-1/2)\,\delta t - \tau)\,d\tau. \qquad (12)$$

The Jacobian matrix is simply given by $J_{\vec{p}}(g) = \tilde{\phi}$, which is independent of the pulse $\vec{p}$.

Importantly, if there are uncertainties in any parameters $\vec{a}$ describing the convolution kernel, so that $\phi(t) = \phi[\vec{a}](t)$, then the objective function used in the optimization routine can be taken as a weighted sum

$$\Phi_{g,\langle \vec{a} \rangle} = \sum_{\vec{a}} \text{Pr}(\vec{a})\Phi_{g[\vec{a}]}, \qquad (13)$$

where $g[\vec{a}](\vec{p}) = \tilde{\phi}[\vec{a}] \cdot \vec{p}$ and the probability distribution $\text{Pr}(\vec{a})$ describes the parameter uncertainty. In this way, the optimizer would attempt to find a solution which performs well over all probable parameter values. As a concrete example, if τ_{rise} were the characteristic rise time of a control amplitude, we could have $\vec{a} = (\tau_{\text{rise}})$, and generate a pulse which is robust to variations in this time scale. By linearity, the Jacobian tensor of $\Phi_{g,\langle \vec{a} \rangle}$, is the weighted sum of the Jacobian tensors $J_{\vec{p}}(g[\vec{a}])$. Incorporating distributions of parameters in the distortion operator, as we will see, applies just as well to nonlinear device hardware.

IV. NONLINEAR CIRCUIT EXAMPLE

As a more involved example than the general linear case described above, we consider a quantum system being controlled by a tuned and matched resonator circuit [53] with nonlinear circuit elements (Fig. 2). We emphasize that while we have picked a relatively simple circuit for this demonstration, it has a general-enough form to accurately describe the majority of resonators used in spin resonance experiments, including the nonlinear resonator described in Ref. [28]. Moreover, arbitrarily complex circuits with additional poles could just as easily be incorporated by finding their circuit equations with a standard application of Kirchhoff's laws, resulting in a higher-order equation in place of Eq. (15).

Nonlinear superconducting resonators are used in a variety of applications, including circuit QED for quantum-information processing and quantum memories [54–56], microwave-kinetic-inductance detectors for astronomy [57], and pulsed electron spin resonance [30–32,58]. Often, however, these devices are operated in their linear regime to avoid complications resulting from nonlinearity. Avoiding nonlinearities requires reducing input power, leading to longer control sequences that reduce the number of quantum operations that can be

$L = 100\text{ pH }(1 + \alpha_L |I_L|^2)$
$R = 0.01\ \Omega\ (1 + \alpha_R |I_L|^{\eta_R})$
$R_L = 50\ \Omega$
$C_t = 2.498\ 21\text{ pF}$
$C_m = 3.582\ 24\text{ fF}$
$\alpha_L = 0.05\text{ A}^{-2}$
$\alpha_R = 0.001\text{ A}^{-2}$
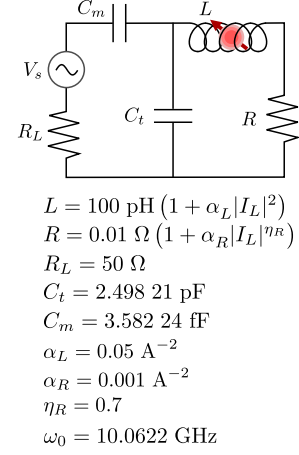$\eta_R = 0.7$
$\omega_0 = 10.0622\text{ GHz}$

FIG. 2. A quantum system being controlled by the magnetic field produced by the inductor of a nonlinear resonator circuit. The ideal voltage source $V_s(t)$ is specified by the input undistorted pulse $\vec{p}$, and the resulting current through the inductor $I_L(t)$ is computed. The inductance and the resistance are both functions of the current passing through them. The form of the nonlinearity is chosen to be consistent with kinetic inductance.

performed before the system decoheres. Additionally, limiting input power removes the natural robustness of high-power sequences to uncertainties in the environment achieved by strongly modulating the quantum system [59,60].

If the circuit were linear, the distortion could be modeled as a convolution $\phi \star$ as discussed above. However, with nonlinear circuit elements present we must numerically solve the circuit's differential equation every time we wish to compute the distorted pulse [27].

As a first demonstration, it is most natural to begin with a qubit system. This is both because it lets us more clearly isolate the change in control landscape induced by the nonlinear distortion operator, and because it is known that control landscapes generally scale well with Hilbert space dimension [61]. Our qubit is a near-resonance spin system whose Hamiltonian, in the rotating frame after invoking the rotating wave approximation, is

$$H = \frac{\delta\omega}{2}\sigma_z + (1 + \kappa)\left(\frac{\omega_x(t)}{2}\sigma_x + \frac{\omega_y(t)}{2}\sigma_y\right), \qquad (14)$$

where $\delta\omega$ and κ represent off-resonance and control power errors, respectively.

The time evolution of the circuit shown in Fig. 2 is governed by the third-order differential equation

$$\frac{d}{dt}\begin{bmatrix} I_L \\ V_{C_m} \\ V_{C_t} \end{bmatrix} = \begin{bmatrix} -\frac{R}{L} & 0 & \frac{1}{L} \\ 0 & \frac{-1}{R_L C_m} & \frac{1}{R_L C_m} \\ \frac{-1}{C_t} & \frac{-1}{R_L C_t} & \frac{1}{R_L C_t} \end{bmatrix}\begin{bmatrix} I_L \\ V_{C_m} \\ V_{C_t} \end{bmatrix} + \begin{bmatrix} 0 \\ \frac{V_s(t)}{R_L C_m} \\ \frac{V_s(t)}{R_L C_t} \end{bmatrix},$$
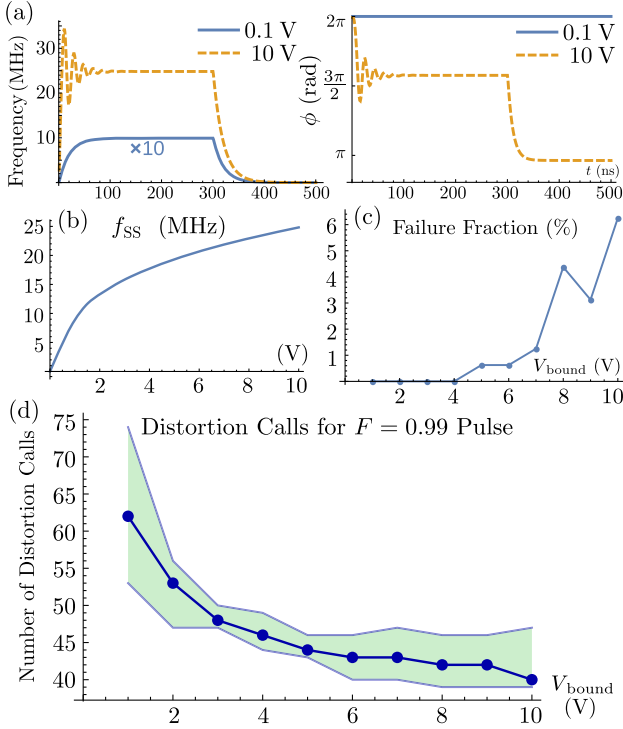
$$(15)$$

FIG. 3. (a) Response from the same resonator to a top-hat input pulse of length 300 ns with an amplitude in both a linear (0.1 V) and nonlinear (10 V) regime. The amplitude of the 0.1-V pulse is multiplied by 10 to make it visible. (b) The steady-state driving frequency as seen by the spins as a function of the voltage input to the resonator. (c) Out of 160 pulses searched for at each of 10 voltage bounds, V_{bound}, with corresponding total pulse length $T_{\mathrm{pulse}} = 0.25/f_{\mathrm{SS}}$, the fraction that failed to reach $F = 0.99$ before the step size was effectively zero. (d) The median number of calls made to the distortion function g along with the 16% and 84% quantiles during the gradient ascent for those pulses which did reach $F = 0.99$.

where the nonlinearities arise when the inductance L and resistance R are functions of the current passing through them [27,62]. In the case of kinetic inductance, these nonlinearities take on the form

$$
\begin{aligned}
L = L(I_L) &= L_0(1 + \alpha_L |I_L|^2), \\
R = R(I_R) &= R_0(1 + \alpha_R |I_R|^\eta),
\end{aligned}
\tag{16}
$$

where α_L, α_R, and η are constants [28,29]. Kinetic inductance leads to a reduction in the circuit resonance frequency, coupling, and quality factor with increasing power, as shown in Figs. 3(a) and 3(b).

Since our Hamiltonian in Eq. (14) is written in a frame rotating at the circuit resonance frequency in the linear regime, it is convenient to write our differential equation in this frame. To this end, with the differential equation (15) shorthanded as $\dot{\vec{y}}(t) = B(\vec{y}(t))\vec{y}(t) + V_s(t)\vec{b}$, we introduce the complex change of variables $\vec{x}(t) = e^{-i\omega_0 t}\vec{y}(t)$. In this

new frame, since $B(\vec{y}(t)) = B(\vec{x}(t))$, our dynamics become

$$
\begin{aligned}
\dot{\vec{x}}(t) &= [B(\vec{x}(t)) - i\omega_0 \mathbb{1}]\vec{x}(t) + \tilde{V}_s(t)\vec{b}, \\
&\equiv A(\vec{x}(t))\vec{x}(t) + \tilde{V}_s(t)\vec{b},
\end{aligned}
\tag{17}
$$

where we have invoked the rotating wave approximation, and $\tilde{V}_s(t)$ is the rotating version of $V_s(t)$. Further details are provided in the Supplemental Material [36], Sec. B. Now the real and imaginary parts of the complex current in the rotating frame, $\tilde{I}_L(t) = e^{-i\omega_0 t}I_L(t)$, are proportional via a geometric factor to the control amplitudes appearing in the Hamiltonian,

$$
\omega_x(t) \propto \mathrm{Re}[\tilde{I}_L(t)] \quad \text{and} \quad \omega_y(t) \propto \mathrm{Im}[\tilde{I}_L(t)].
\tag{18}
$$

To compute the distortion $\vec{q} = g(\vec{p})$ caused by the resonator, we set the circuit's input voltage $\tilde{V}_s(t)$ to be the piecewise constant function with amplitudes coming from $\vec{p}$. To improve stiffness conditions, a small finite rise time may be added to the forcing term $\tilde{V}_s(t)$, which is equivalent to adding a low-pass filter to the ideal voltage source in the circuit. We can now solve Eqs. (17) for $\tilde{I}_L(t)$ using the NDSOLVE function in *Mathematica 10*, interpolate the results, and resample at a rate δt to determine the distorted pulse $\vec{q}$.

Because our distortion is nonlinear, the Jacobian of g will not be constant with respect to the input pulse $\vec{p}$. However, we may compromise the accuracy of the Jacobian in favor of taking a larger number of ascent steps that are still generally uphill by using the approximation

$$
\left.\frac{\partial g_{m,l}}{\partial p_{n,k}}\right|_{\vec{p}} \approx [g(\epsilon \vec{e}_{n,k})/\epsilon]_{m,l}.
\tag{19}
$$

These quantities may be precomputed prior to gradient ascent and therefore only add a constant to the computation time. Exact partial derivatives may be computed for a cost that scales as KN and whose implementation can be highly parallelized, as derived in the Supplemental Material [36], Sec. C2.

In Fig. 4, we show an example of a GRAPE-optimized pulse for $U = \pi/2)_x$, with the circuit of Fig. 2 used as a distortion operator. There are 16 time steps of length 0.5 ns shown as a solid-red step function. The pulse has been made to be robust to static uncertainty in the Hamiltonian parameters $\delta\omega$ and γ and the nonlinearity parameter α_L. Since the circuit has a high quality factor, it would take many times the length of the pulse for the ringdown tail to decay to zero. We therefore utilize an active ringdown suppression scheme with three compensation steps of lengths 4, 2, and 1 ns. This is a generalization of ringdown
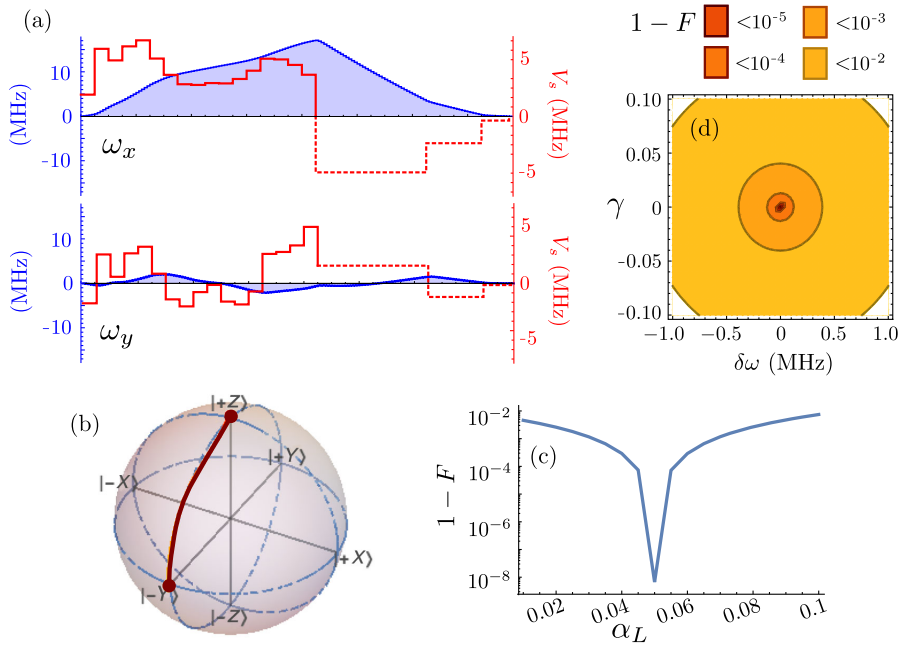
FIG. 4. (a) Example of a $\pi/2)_x$ pulse generated for the matched nonlinear resonator circuit. The driving term ($\vec{p}$) is shown in red, while the distorted pulse ($\vec{q}$) is shown in blue. The dashed segments are the ringdown compensation steps. (b) The trajectory of the state $|0\rangle$ under this pulse is shown on the Bloch sphere, and (c),(d) the average fidelity is plotted for different values of α_L, $\delta\omega$, and γ.

suppression in linear circuits [13,63,64] with details presented in the Supplemental Material [36], Sec. D.

Having demonstrated the ability to find a robust gate in the presence of our nonlinear distortion operator, we now study the effect it has on the control landscape. It would perhaps be anticipated that, in the presence of a nontrivial distortion operator, finding optimal solutions would become more expensive, measured in the number of steps taken by the optimizer. Therefore, a trade-off between computational cost and gate-time length could reasonably be expected. We perform a numerical study to examine this relationship.

We bound the allowed input power to the resonator used by the GRAPE algorithm by ten different voltages, 1 to 10 V, where 1 V is on the edge of the linear regime and 10 V is highly nonlinear. In analogy to the numerical control-landscape experiments performed in Ref. [48], for each of these bounds, we attempt to compute a fidelity $F = 0.99$ $\pi/2)_x$ pulse 160×, with a different random initial guess each time. The total length of the pulse is set to $T_{\text{pulse}} = 0.25/f_{\text{SS}}$ where f_{SS} is the steady-state driving frequency of the resonator at the corresponding voltage bound. The number of time steps is held constant at $N = 16$ for each trial. The gradient approximation from Eq. (19) is used. On each trial, we count the number of times the distortion function g is called. The results are shown in Fig. 3, where it is seen that the number of calls actually tends to decrease as the allowed nonlinearity is increased, indicating that the control landscape does not become more difficult to navigate.

V. CONCLUSION

In conclusion, we have presented an optimization framework that permits the design of robust quantum control sequences that account for general simulatable distortions by classical control hardware. We have demonstrated that even when distortions are nonlinear with respect to the input—using the particular example of a nonlinear resonator circuit—robust quantum control may still be achieved, and searching through the control landscape does not necessarily become more difficult. Thus, classical control devices may be operated in their high-power regime to permit fast high-fidelity quantum operations, increasing the number of gates that can be performed within the decoherence time of the quantum system.

[1] T. D. Ladd, F. Jelezko, R. Laflamme, Y. Nakamura, C. Monroe, and J. L. OBrien, Quantum computers, Nature (London) **464**, 45 (2010).
[2] J. S. Hodges, J. C. Yang, C. Ramanathan, and D. G. Cory, Universal control of nuclear spins via anisotropic hyperfine interactions, Phys. Rev. A **78**, 010303 (2008).
[3] T. W. Borneman, C. E. Granade, and D. G. Cory, Parallel Information Transfer in a Multinode Quantum Information Processor, Phys. Rev. Lett. **108**, 140502 (2012).
[4] P. Cappellaro, J. Emerson, N. Boulant, C. Ramanathan, S. Lloyd, and D. G. Cory, Entanglement Assisted Metrology, Phys. Rev. Lett. **94**, 020502 (2005).
[5] H. J. Mamin, M. Kim, M. H. Sherwood, C. T. Rettner, K. Ohno, D. D. Awschalom, and D. Rugar, Nanoscale nuclear

magnetic resonance with a nitrogen-vacancy spin sensor, Science **339**, 557 (2013).

[6] J. M. Taylor, P. Cappellaro, L. Childress, L. Jiang, D. Budker, P. R. Hemmer, A. Yacoby, R. Walsworth, and M. D. Lukin, High-sensitivity diamond magnetometer with nanoscale resolution, Nat. Phys. **4**, 810 (2008).

[7] Daniel Gottesman, An introduction to quantum error correction and fault-tolerant quantum computation, arXiv:0904.2557.

[8] Austin G. Fowler, Ashley M. Stephens, and Peter Groszkowski, High-threshold universal quantum computation on the surface code, Phys. Rev. A **80**, 052312 (2009).

[9] Mauricio Gutierrez, Lukas Svec, Alexander Vargo, and Kenneth R. Brown, Approximation of realistic errors by Clifford channels and Pauli measurements, Phys. Rev. A **87**, 030302 (2013).

[10] R. Tycko, Broadband Population Inversion, Phys. Rev. Lett. **51**, 775 (1983).

[11] S. Wimperis, Broadband, narrowband, and passband composite pulses for use in advanced NMR experiments, J. Magn. Reson., Ser. A **109**, 221 (1994).

[12] Benjamin Rowland and Jonathan A. Jones, Implementing quantum logic gates with gradient ascent pulse engineering: Principles and practicalities, Phil. Trans. R. Soc. A **370**, 4636 (2012).

[13] Troy W. Borneman and David G. Cory, Bandwidth-limited control and ringdown suppression in high-Q resonators, J. Magn. Reson. **225**, 120 (2012).

[14] Philipp E. Spindler, Yun Zhang, Burkhard Endeward, Naum Gershernzon, Thomas E. Skinner, Steffen J. Glaser, and Thomas F. Prisner, Shaped optimal control pulses for increased excitation bandwidth in EPR, J. Magn. Reson. **218**, 49 (2012).

[15] Georg Jger and Ulrich Hohenester, Optimal quantum control of Bose-Einstein condensates in magnetic microtraps: Consideration of filter effects, Phys. Rev. A **88**, 035601 (2013).

[16] F. Motzoi, J. M. Gambetta, S. T. Merkel, and F. K. Wilhelm, Optimal control methods for rapidly time-varying Hamiltonians, Phys. Rev. A **84**, 022307 (2011).

[17] Lev Semenovich Pontryagin, *Mathematical Theory of Optimal Processes* (CRC Press, Boca Raton, 1987).

[18] Navin Khaneja, Timo Reiss, Cindie Kehlet, Thomas Schulte-Herbrggen, and Steffen J. Glaser, Optimal control of coupled spin dynamics: Design of NMR pulse sequences by gradient ascent algorithms, J. Magn. Reson. **172**, 296 (2005).

[19] Kyryl Kobzar, Sebastian Ehni, Thomas E. Skinner, Steffen J. Glaser, and Burkhard Luy, Exploring the limits of broadband 90 and 180 universal rotation pulses, J. Magn. Reson. **225**, 142 (2012).

[20] Van D. M. Koroleva, Soumyajit Mandal, Yi-Qiao Song, and Martin D. Hürlimann, Broadband CPMG sequence with short composite refocusing pulses, J. Magn. Reson. **230**, 64 (2013).

[21] Troy W. Borneman, Martin D. Hürlimann, and David G. Cory, Application of optimal control to CPMG refocusing pulse design, J. Magn. Reson. **207**, 220 (2010).

[22] Soumyajit Mandal, Van D. M. Koroleva, Troy W. Borneman, Yi-Qiao Song, and Martin D. Hürlimann, Axis-matching excitation pulses for CPMG-like sequences in inhomogeneous fields, J. Magn. Reson. **237**, 1 (2013).

[23] Soumyajit Mandal, Troy W. Borneman, Van D. M. Koroleva, and Martin D. Hürlimann, Direct optimization of signal-to-noise ratio of CPMG-like sequences in inhomogeneous fields, J. Magn. Reson. **247**, 54 (2014).

[24] T. Schulte-Herbrggen, A. Sprl, N. Khaneja, and S. J. Glaser, Optimal control for generating quantum gates in open dissipative systems, J. Phys. B **44**, 154013 (2011).

[25] Michael H. Goerz, Daniel M. Reich, and Christiane P. Koch, Optimal control theory for a unitary operation under dissipative evolution, New J. Phys. **16**, 055012 (2014).

[26] D. J. Egger and F. K. Wilhelm, Adaptive Hybrid Optimal Quantum Control for Imprecisely Characterized Systems, Phys. Rev. Lett. **112**, 240503 (2014).

[27] Stephen A. Maas, *Nonlinear Microwave and RF Circuits* (Artech House Publishers, Boston, MA, 2003).

[28] H. R. Mohebbi, O. W. B. Benningshof, I. A. J. Taminiau, G. X. Miao, and D. G. Cory, Composite arrays of superconducting microstrip line resonators, J. Appl. Phys. **115**, 094502 (2014).

[29] T. Dahm and D. J. Scalapino, Theory of intermodulation in a superconducting microstrip resonator, J. Appl. Phys. **81**, 2002 (1997).

[30] O. W. B. Benningshof, H. R. Mohebbi, I. A. J. Taminiau, G. X. Miao, and D. G. Cory, Superconducting microstrip resonator for pulsed ESR of thin films, J. Magn. Reson. **230**, 84 (2013).

[31] H. Malissa, D. I. Schuster, A. M. Tyryshkin, A. A. Houck, and S. A. Lyon, Superconducting coplanar waveguide resonators for low temperature pulsed electron spin resonance spectroscopy, Rev. Sci. Instrum. **84**, 025116 (2013).

[32] A. J. Sigillito, H. Malissa, A. M. Tyryshkin, H. Riemann, N. V. Abrosimov, P. Becker, H.-J. Pohl, M. L. W. Thewalt, K. M. Itoh, J. J. L. Morton, A. A. Houck, D. I. Schuster, and S. A. Lyon, Fast, low-power manipulation of spin ensembles in superconducting microresonators, Appl. Phys. Lett. **104**, 222407 (2014).

[33] Gershon Kurizki, Patrice Bertet, Yuimaru Kubo, Klaus Mlmer, David Petrosyan, Peter Rabl, and Jrg Schmiedmayer, Quantum technologies with hybrid systems, Proc. Natl. Acad. Sci. U.S.A. **112**, 3866 (2015).

[34] Ze-Liang Xiang, Sahel Ashhab, J. Q. You, and Franco Nori, Hybrid quantum circuits: Superconducting circuits interacting with other quantum systems, Rev. Mod. Phys. **85**, 623 (2013).

[35] Domenico d'Alessandro, *Introduction to Quantum Control and Dynamics* (CRC Press, Boca Raton, Florida, 2007).

[36] See Supplemental Material at http://link.aps.org/supplemental/10.1103/PhysRevApplied.4.024012, which includes Refs. [37,38], for further examples of distortions, their derivations, and the details of ringdown suppression in nonlinear circuits.

[37] S. Gustavsson, O. Zwier, J. Bylander, F. Yan, F. Yoshihara, Y. Nakamura, T. P. Orlando, and W. D. Oliver, Improving Quantum Gate Fidelities by Using a Qubit to Measure

Microwave Pulse Distortions, Phys. Rev. Lett. **110**, 040502 (2013).

[38] M. H. Levitt, *Spin Dynamics: Basics of Nuclear Magnetic Resonance* (Wiley, Chichester, 2001).

[39] P. de Fouquieres, S. G. Schirmer, S. J. Glaser, and Ilya Kuprov, Second order gradient ascent pulse engineering, J. Magn. Reson. **212**, 412 (2011).

[40] Shai Machnes, David J. Tannor, Frank K. Wilhelm, and Elie Assmat, Gradient optimization of analytic controls: The route to high accuracy quantum optimal control, arXiv:1507.04261.

[41] Michael H. Goerz, K. Birgitta Whaley, and Christiane P. Koch, Hybrid optimization schemes for quantum control, arXiv:1505.05331.

[42] David Hocker, Constantin Brif, Matthew D. Grace, Ashley Donovan, Tak-San Ho, Katharine W. Moore Tibbetts, Rebing Wu, and Herschel Rabitz, Characterization of control noise effects in optimal quantum unitary dynamics, Phys. Rev. A **90**, 062309 (2014).

[43] Thomas E. Skinner, Timo O. Reiss, Burkhard Luy, Navin Khaneja, and Steffen J. Glaser, Reducing the duration of broadband excitation pulses using optimal control with limited RF amplitude, J. Magn. Reson. **167**, 68 (2004).

[44] Kyryl Kobzar, Thomas E. Skinner, Navin Khaneja, Steffen J. Glaser, and Burkhard Luy, Exploring the limits of broadband excitation and inversion: II. Rf-power optimized pulses, J. Magn. Reson. **194**, 58 (2008).

[45] Jos P. Palao, Ronnie Kosloff, and Christiane P. Koch, Protecting coherence in optimal control theory: State-dependent constraint approach, Phys. Rev. A **77**, 063412 (2008).

[46] M. M. Müller, D. M. Reich, M. Murphy, H. Yuan, J. Vala, K. B. Whaley, T. Calarco, and C. P. Koch, Optimizing entangling quantum gates for physical systems, Phys. Rev. A **84**, 042315 (2011).

[47] Christopher Wood, Ian Hincks, and Christopher Granade, QUANTUMUTILS for Mathematica, 2015.

[48] Katharine Moore, Michael Hsieh, and Herschel Rabitz, On the relationship between quantum control landscape structure and optimization complexity, J. Chem. Phys. **128**, 154117 (2008).

[49] J. A. Nelder and R. Mead, A simplex method for function minimization, Comput. J. **7**, 308 (1965).

[50] Christopher E. Granade, Characterization, verification and control for large quantum systems, Ph.D. thesis, University of Waterloo, Waterloo, ON, Canada, 2015.

[51] Douglas D. Rife and John Vanderkooy, Transfer-function measurement with maximum-length sequences, J. Audio Eng. Soc. **37**, 419 (1989).

[52] R. Barends, J. Kelly, A. Megrant, A. Veitia, D. Sank, E. Jeffrey, T. C. White, J. Mutus, A. G. Fowler, B. Campbell, Y. Chen, Z. Chen, B. Chiaro, A. Dunsworth, C. Neill, P. OMalley, P. Roushan, A. Vainsencher, J. Wenner, A. N. Korotkov, A. N. Cleland, and John M. Martinis, Superconducting quantum circuits at the surface code threshold for fault tolerance, Nature (London) **508**, 500 (2014).

[53] Thomas M. Barbara, Joel F. Martin, and Jon G. Wurl, Phase transients in NMR probe circuits, J. Magn. Reson. (1969) **93**, 497 (1991).

[54] R. J. Schoelkopf and S. M. Girvin, Wiring up quantum systems, Nature (London) **451**, 664 (2008).

[55] S. Putz, D. O. Krimer, R. Amsss, A. Valookaran, T. Nbauer, J. Schmiedmayer, S. Rotter, and J. Majer, Protecting a spin ensemble against decoherence in the strong-coupling regime of cavity QED, Nat. Phys. **10**, 720 (2014).

[56] C. Grezes, B. Julsgaard, Y. Kubo, M. Stern, T. Umeda, J. Isoya, H. Sumiya, H. Abe, S. Onoda, T. Ohshima, V. Jacques, J. Esteve, D. Vion, D. Esteve, K. Mølmer, and P. Bertet, Multimode Storage and Retrieval of Microwave Fields in a Spin Ensemble, Phys. Rev. X **4**, 021049 (2014).

[57] Peter K. Day, Henry G. LeDuc, Benjamin A. Mazin, Anastasios Vayonakis, and Jonas Zmuidzinas, A broadband superconducting detector suitable for use in large arrays, Nature (London) **425**, 817 (2003).

[58] Gil Bachar, Oren Suchoi, Oleg Shtempluck, Aharon Blank, and Eyal Buks, Nonlinear induction detection of electron spin resonance, Appl. Phys. Lett. **101**, 022602 (2012).

[59] Evan M. Fortunato, Marco A. Pravia, Nicolas Boulant, Grum Teklemariam, Timothy F. Havel, and David G. Cory, Design of strongly modulating pulses to implement precise effective Hamiltonians for quantum information processing, J. Chem. Phys. **116**, 7599 (2002).

[60] Marco A. Pravia, Nicolas Boulant, Joseph Emerson, Amro Farid, Evan M. Fortunato, Timothy F. Havel, R. Martinez, and David G. Cory, Robust control of quantum information, J. Chem. Phys. **119**, 9993 (2003).

[61] Herschel A. Rabitz, Michael M. Hsieh, and Carey M. Rosenthal, Quantum optimally controlled transition landscapes, Science **303**, 1998 (2004).

[62] Michael Tinkham, *Introduction to Superconductivity* (Dover Publications, Mineola, NY, 2004).

[63] Michael Mehring, *Principles of High Resolution NMR in Solids* (Springer, Berlin, 1976).

[64] D. I. Hoult, Fast recovery, high sensitivity NMR probe and preamplifier for low frequencies, Rev. Sci. Instrum. **50**, 193 (1979).